J|A|C|S ARTICLES

Published on Web 10/28/2010

Designing Multifunctional Expanded Pyridiniums: Properties of Branched and Fused Head-to-Tail Bipyridiniums

Jérôme Fortage,[†,‡] Cyril Peltier,[§] Francesco Nastasi,[||] Fausto Puntoriero,[||] Fabien Tuyèras,[†] Sophie Griveau,[⊥] Fethi Bedioui,[⊥] Carlo Adamo,[§] Ilaria Ciofini,*[,§] Sebastiano Campagna,*[,||] and Philippe P. Lainé*[,†]

Laboratoire de Chimie et Biochimie Pharmacologiques et Toxicologiques (CNRS UMR-8601), Université Paris Descartes, 45 rue des Saints Pères, F-75270 Paris Cedex 06, France, Institut Parisien de Chimie Moléculaire (CNRS UMR-7201), Equipe Chimie Supramoléculaire, Case 42, Université Pierre et Marie Curie, 4 Place Jussieu, 75252 Paris Cedex 05, France, LECIME, Laboratoire d'Électrochimie, Chimie des Interfaces et Modélisation pour l'Énergie (CNRS UMR-7575), École Nationale Supérieure de Chimie de Paris-Chimie ParisTech, 11 rue Pierre et Marie Curie, F-75231 Paris Cedex 05, France, Dipartimento di Chimica Inorganica, Chimica Analitica e Chimica Fisica and Centro Interuniversitario per la Conversione Chimica dell'Energia Solare, Università di Messina, Via Sperone 31, I-98166 Messina, Italy, and Laboratoire de Pharmacologie Chimique et Génétique (CNRS UMR-8151 and INSERM U-1022), Université Paris Descartes, École Nationale Supérieure de Chimie de Paris-Chimie ParisTech, 11 rue Pierre et Marie Curie, F-75231 Paris Cedex 05, France

Received September 25, 2010; E-mail: philippe.laine@parisdescartes.fr; campagna@unime.it; ilaria-ciofini@chimie-paristech.fr

Abstract: The multifaceted potentialities of expanded pyridiniums (EPs), based on one pyridinium core bearing a 4-pyridyl or 4-pyridylium as the *N*-pyridinio group, are established at both experimental and theoretical levels. Two classes of head-to-tail (*htt*) EPs were designed, and their first representative elements were synthesized and fully characterized. The branched (B) family is made up of 2,6-diphenyl-4-aryl-1,4′-bipyridin-1-ium (or 1,1′-diium) species, denoted **1B** and **2B** for monocationic EPs (with aryl = phenyl and biphenyl, respectively) and $\mathbf{1B_{Me}}$ and $\mathbf{2B_{Me}}$ for related quaternarized dicationic species. The series of fused (F) analogues comprises 9-aryl-benzo[*c*]benzo[1,2]quinolizino[3,4,5,6-*ija*][1,6]naphthyridin-15-ium species, denoted **1F** and **2F**, and their 2,15-diium derivatives referred to as $\mathbf{1F_{Me}}$ and $\mathbf{2F_{Me}}$. Electrochemistry (in MeCN vs SCE) reveals that branched EPs undergo a single reversible bielectronic reduction at ca. −0.92 V for **1B**/**2B** and −0.59 V for $\mathbf{1B_{Me}}$/$\mathbf{2B_{Me}}$, whereas pericondensed species show two reversible monoelectronic reductions at ca. −0.83 and −1.59 V for **1F**/**2F** and ca. −0.42 and −1.07 V for $\mathbf{1F_{Me}}$/$\mathbf{2F_{Me}}$. Regarding electronic absorption features, all *htt*-EP chromophores show absorptivity in the range of ca. $1-4 \times 10^4$ M^{-1} cm^{-1}, with red-edge absorptions extending toward 450 and 500 nm (in MeCN) for $\mathbf{2B_{Me}}$ and $\mathbf{2F_{Me}}$, respectively. These lowest-energy pi−pi* transitions are ascribed to intramolecular charge transfer between the electron-releasing biphenyl group and the *htt*-bipyridinium electron-withdrawing subsystems. EPs display room-temperature photoemission quantum yields ranging from 10% to 50%, with the exception of **1B**, and branched luminophores are characterized by larger Stokes shifts (8000−10 000 cm^{-1}) than fused ones. Lastly, a method to predict the efficiency of photobiscyclization of branched EPs into fused ones, based on the analysis of computed difference maps in total electron density for singlet excited states, is proposed.

1. Introduction

Pyridinium and bipyridinium[1] species are among the most extensively used functional entities[2,3] because of their appealing electron-withdrawing (pull effect)[4,5] and electron-accepting (redox)[6,7] properties. By virtue of their reduction properties they are suited to artificial systems developed for solar energy conversion, both in bimolecular schemes and in supramolecular (multicomponent) arrangements in which they play the role of electron acceptors (i.e., electrophores).[8] Their mild and reversible reduction processes also make them choice components in supramolecular assemblies designed to behave as electron-storage systems (e.g., polyviologen dendrimers)[9,10] or molecular machines[11,12] whose organization and machinery are based on charge-transfer interactions and redox inputs, respectively.[3,13]

[†] LCBPT-Université Paris Descartes.
[‡] IPCM-Université Pierre et Marie Curie.
[§] LECIME-ENSCP.
[||] Università di Messina.
[⊥] LPCG-ENSCP-Université Paris Descartes.

(1) Sliwa, W. *Curr. Org. Chem.* **2003**, *7*, 995–1048.

(2) When performing a bibliometric analysis through the ISI Web of Knowledge, a striking point is the close correlation observed in the evolution over the years of the number of publications (and related citations) dealing with the following topics: "viologen" or "bipyridinium" and "ruthenium bipyridine". Two remarkable inflection points are found around 1980 and 1990. They are ascribable to the launching of two related topics: "water splitting" and "artificial photosynthesis", on the one hand, and "molecular devices" including "molecular machines", on the other; see also ref 3.

(3) Balzani, V.; Bergamini, G.; Ceroni, P. *Coord. Chem. Rev.* **2008**, *252*, 2456–2469.

 10.1021/ja108668h

Pyridinium species, already known for their redox properties as electrophores, have also attracted attention for their electro-optical and photophysical properties.[14−19] Indeed, there is great interest in designing new types of pyridiniums that behave not only as good electrophores but also as luminophores and chromophores, that is, as truly multifunctional and polyvalent entities. Efforts in this direction may go through the expansion of the molecular scaffold of pyridiniums[20] and, in particular, of their π system.[21] Similarly to macromolecular unsaturated hydrocarbon architectures in which connecting patterns[22] are based on (i) single-bond linkages and/or (ii) edge-fused linkages, skeletal expansion of pyridiniums can take the form of aryl-substituted[23,24] and pericondensed[16] species, hereafter referred to as branched (B) and fused (F) expanded pyridiniums (EPs), respectively (Chart 1).

Chart 1. General Representation of Tetra- (**TP**)[23,24] and Hexabranched (**XP**) EPs of the First Generation along with Corresponding Fused (***f*TP**) and Hemi-Fused (***hf*XP**) EPs[16]

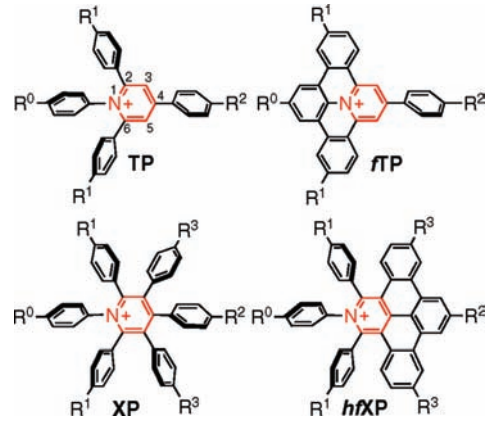

The approach adopted here to design integrated multifunctional EPs consists in close redox tuning,[6,7] combined with a strategy relying on the extension of the π-conjugated system of pyridiniums for absorption and emission properties.

Indeed, our previous investigations on EPs of the first generation (Chart 1)[16,23,24] established that the electronic, photophysical, and electrochemical properties of pyridiniums are all significantly affected by scaffold expansion (whether by

(4) For selected references dealing with pyridinium-based solvatochromic dyes, see:(a) Reichardt, C. *Chem. Rev.* **1994**, *94*, 2319–2358, and references therein. (b) Chen, P.; Meyer, T. J. *Chem. Rev.* **1998**, *98*, 1439–1477. (c) Narang, U.; Zhao, C. F.; Bhawalkar, J. D.; Bright, F. V.; Prasad, P. N. *J. Phys. Chem.* **1996**, *100*, 4521–4525.

(5) For purely organic pyridinium-based molecules showing a nonlinear optical (NLO) activity, see for instance: (a) Marder, S. R.; Perry, J. W.; Yakymyshyn, C. P. *Chem. Mater.* **1994**, *6*, 1137–1147. (b) Marder, S. R.; Perry, J. W.; Schaefer, W. P. *Science* **1989**, *245*, 626–628. For inorganic NLO-phores, see, for instance: (c) Coe, B. J. *Acc. Chem. Res.* **2006**, *39*, 383–393. (d) Konstantaki, M.; Koudoumas, E.; Couris, S.; Lainé, P.; Amouyal, E.; Leach, S. *J. Phys. Chem. B* **2001**, *105*, 10797–10804. (e) Marder, S. R.; Perry, J. W.; Tiemann, B. G.; Schaefer, W. P. *Organometallics* **1991**, *10*, 1896–1901.

(6) Hünig, S.; Berneth, H. *Top. Curr. Chem.* **1980**, *92*, 1–44.

(7) Bird, C. L.; Kuhn, A. T. *Chem. Soc. Rev.* **1981**, *10*, 49–82.

(8) There are literally hundreds of examples of papers where pyridinium and/or bipyridinium species act as electron acceptors in photoinduced electron transfer processes. For a few selected early and/or seminal and/or influential contributions involving bipyridiniums, see the following references. Topic of prototypical photochemistry of the ruthenium(II) tris(2,2′-bipyridine) complex with the 1,1′-dimethyl-4,4′-bipyridinium electron-accepting quencher: (a) Bock, C. R.; Meyer, T. J.; Whitten, D. G. *J. Am. Chem. Soc.* **1974**, *96*, 4710–4712. (b) Whitten, D. G. *Acc. Chem. Res.* **1980**, *13*, 83–90. (c) Juris, A.; Balzani, V.; Barigelletti, F.; Campagna, S.; Belser, P.; Von Zelewsky, A. *Coord. Chem. Rev.* **1988**, *84*, 85–277. Topic of photochemical solar energy conversion: (d) Balzani, V.; Moggi, L.; Manfrin, M. F.; Bolletta, F.; Gleria, M. *Science* **1975**, *189*, 852–856. (e) Young, R. C.; Meyer, T. J.; Whitten, D. G. *J. Am. Chem. Soc.* **1975**, *97*, 4781–4782. (f) Grätzel, M. *Acc. Chem. Res.* **1981**, *14*, 376–384. (g) Kalyanasundaram, K. *Coord. Chem. Rev.* **1982**, *46*, 159–244. Topic of multimolecular systems for hydrogen evolution: (h) Lehn, J.-M.; Sauvage, J.-P. *Nouv. J. Chim.* **1977**, *1*, 449–451. (i) Moradpour, A.; Amouyal, E.; Keller, P.; Kagan, H. *Nouv. J. Chim.* **1978**, *2*, 547–549. (j) Kalyanasundaram, K.; Kiwi, J.; Grätzel, M. *Helv. Chim. Acta* **1978**, *61*, 2720–2730. (k) Harriman, A.; Porter, G. *J. Chem. Soc., Faraday Trans. 2* **1982**, *78*, 1937–1943. Topic of photochemical devices (PMDs) in the field of supramolecular photochemistry: (l) Balzani, V. *Tetrahedron* **1992**, *48*, 10443–10514. (m) Balzani, V.; Scandola, F. *Supramolecular Photochemistry*; Ellis Horwood: Chichester, U.K., 1991; Chapter *12*. (n) Balzani, V.; Moggi, L.; Scandola, F. In *Supramolecular Photochemistry*; Balzani, V., Ed.; D. Reidel Publishing Co.: Dordrecht, The Netherlands, 1987; pp 1−28. Topic of integrated supramolecular functional assemblies devoted to artificial photosynthesis: (o) Meyer, T. J. *Acc. Chem. Res.* **1989**, *22*, 163–170. (p) Sauvage, J.-P.; Collin, J.-P.; Chambron, J.-C.; Guillerez, S.; Coudret, C.; Balzani, V.; Barigelletti, F.; De Cola, L.; Flamigni, L. *Chem. Rev.* **1994**, *94*, 993–1019. (q) Yonemoto, E. H.; Riley, R. L.; Il Kim, Y.; Atherton, S. J.; Schmehl, R. H.; Mallouk, T. E. *J. Am. Chem. Soc.* **1992**, *114*, 8081–8087. (r) Dürr, H.; Bossmann, S. *Acc. Chem. Res.* **2001**, *34*, 905–917.

(9) Ronconi, C. M.; Stoddart, J. F.; Balzani, V.; Baroncini, M.; Ceroni, P.; Giansante, C.; Venturi, M. *Chem.—Eur. J.* **2008**, *14*, 8365–8373.

(10) (a) Juris, A. *Annu. Rep. Prog. Chem., Sect. C* **2003**, *99*, 177–241. (b) Toba, R.; Quintela, J. M.; Peinador, C.; Roman, E.; Kaifer, A. E. *Chem. Commun.* **2002**, 1768–1769. (c) Baker, W. S.; Lemon, B. I., III; Crooks, R. M. *J. Phys. Chem. B* **2001**, *105*, 8885–8894. (d) Ceroni, P.; Venturi, M. In *Electrochemistry of Functional Supramolecular Systems*; Ceroni, P., Credi, A., Venturi, M., Eds.; Wiley: Hoboken, NJ, 2010; pp 145−184.

(11) Sliwa, W.; Bachowska, B.; Girek, T. *Curr. Org. Chem.* **2007**, *11*, 497–513.

(12) For selected early works in the field, see: (a) Anelli, P. L.; Spencer, N.; Stoddart., J. F. *J. Am. Chem. Soc.* **1991**, *113*, 5131–5133. (b) Anelli, P. L.; et al. *J. Am. Chem. Soc.* **1992**, *114*, 193–218. (c) Ballardini, R.; Balzani, V.; Gandolfi, M. T.; Prodi, L.; Venturi, M.; Philp, D.; Ricketts, H. G.; Stoddart, J. F. *Angew. Chem., Int. Ed. Engl.* **1993**, *32*, 1301–1303. (d) Balzani, V.; Gomez-Lopez, M.; Stoddart, J. F. *Acc. Chem. Res.* **1998**, *31*, 405–414.

(13) Credi, A.; Venturi, M. In *Electrochemistry of Functional Supramolecular Systems*; Ceroni, P., Credi, A., Venturi, M., Eds.; Wiley: Hoboken, NJ, 2010; pp 377−424 and references therein.

(14) Knyazhanskii, M. I.; Tymyanskii, Y. R.; Feigelman, V. M.; Katritzky, A. R. *Heterocycles* **1987**, *26*, 2963–2982.

(15) Peltier, C.; Lainé, P. P.; Scalmani, G.; Frisch, M. J.; Adamo, C.; Ciofini, I. *J. Mol. Struct.: THEOCHEM* **2009**, *914*, 94–99.

(16) Fortage, J.; Tuyèras, F.; Ochsenbein, P.; Puntoriero, F.; Nastasi, F.; Campagna, S.; Griveau, S.; Bedioui, F.; Ciofini, I.; Lainé, P. P. *Chem.—Eur. J.* **2010**, *16*, 11047–11063.

(17) Peltier, C.; Adamo, C.; Lainé, P. P.; Campagna, S.; Puntoriero, F.; Ciofini, I. *J. Phys. Chem. A* **2010**, *114*, 8434–8443.

(18) Balzani, V.; Credi, A.; Langford, S. J.; Prodi, A.; Stoddart, J. F.; Venturi, M. *Supramol. Chem.* **2001**, *13*, 303–311.

(19) Ballardini, R.; Credi, A.; Gandolfi, M. T.; Giansante, C.; Marconi, G.; Silvi, S.; Venturi, M. *Inorg. Chim. Acta* **2007**, *360*, 1072–1082.

(20) Arai, S.; Hida, M. *Adv. Heterocycl. Chem.* **1992**, *55*, 261–358.

(21) Bendikov, M.; Wudl, F.; Perepichka, D. F. *Chem. Rev.* **2004**, *104*, 4891–4945, and references therein.

(22) (a) Müller, S.; Müllen, K. *Phil. Trans. R. Soc. A* **2007**, *365*, 1453–1472. (b) Watson, M. D.; Fechtenkötter, A.; Müllen, K. *Chem. Rev.* **2001**, *101*, 1267–1300.

(23) (a) Lainé, P.; Bedioui, F.; Ochsenbein, P.; Marvaud, V.; Bonin, M.; Amouyal, E. *J. Am. Chem. Soc.* **2002**, *124*, 1364–1377. (b) Lainé, P.; Bedioui, F.; Amouyal, E.; Albin, V.; Berruyer-Penaud, F. *Chem.—Eur. J.* **2002**, *8*, 3162–3176. (c) Lainé, P.; Amouyal, E. *Chem. Commun.* **1999**, 935–936.

(24) (a) Lainé, P. P.; Campagna, S.; Loiseau, F. *Coord. Chem. Rev.* **2008**, *252*, 2552–2571. (b) Lainé, P. P.; Bedioui, F.; Loiseau, F.; Chiorboli, C.; Campagna, S. *J. Am. Chem. Soc.* **2006**, *128*, 7510–7521. (c) Lainé, P. P.; Loiseau, F.; Campagna, S.; Ciofini, I.; Adamo, C. *Inorg. Chem.* **2006**, *45*, 5538–5551. (d) Lainé, P. P.; Ciofini, I.; Ochsenbein, P.; Amouyal, E.; Adamo, C.; Bedioui, F. *Chem.—Eur. J.* **2005**, *11*, 3711–3727. (e) Ciofini, I.; Lainé, P. P.; Bedioui, F.; Adamo, C. *J. Am. Chem. Soc.* **2004**, *126*, 10763–10777.

ring branching[16,23,24] or by ring fusion[16]). Yet, these properties are impacted differently when passing from branched to corresponding fused molecular backbones (Chart 1).[16] On the one hand, the two types of EPs exhibit distinct electronic and photophysical characteristics, i.e., they are basically different chromophores and luminophores. On the other hand, their redox properties barely change when aryl branches are pericondensed, especially for the potential of the first reduction process (E_{red}). This finding was ascribed to the fact that beyond substituent effects attached to aryl appending (for branched EPs) and ring fusion (e.g., benzoannulation in fused EPs), the features of the LUMO are essentially the same in both types of EPs. In addition, they are closely akin to those of the bare *N*-methylpyridinum.[17] In other words, in the case of monopyridinium derivatives, the LUMO remains essentially localized on the pyridinium motif regardless of the type of skeletal expansion, including the extension of the π-conjugated system by pericondensation of branched EPs.[16,17]

Expanding the molecular scaffold of pyridiniums by extending their π-conjugated system is an efficient means to modify their electronic and photophysical features to obtain good pyridinium-based chromophores and luminophores. Yet, it is an inoperative approach to control their electrochemical properties (especially in the reduction regime).[16,17] Therefore, improving the electrophoric properties of pyridiniums, that is, obtaining the anodic shift of their first reduction potential to make these EPs more easily reducible, must somehow rely on pyridinium substitution with electron-withdrawing groups. Unfortunately, in spite of the great chemical versatility of EPs of the first generation (R^n substituents in Chart 1)[23] peripheral substitution failed in rendering thus-modified monopyridinium species competitive with other electron acceptors commonly exploited to efficiently monitor photoinduced electron transfers ($E_{red} \geq -0.6$ V vs SCE).[24] With regard to branched EPs, this failure was observed even in the favorable cases of aryl branches that are (i) para substituted with strongly electron-withdrawing nitro groups and (ii) appended at the most influential C-2, C-4, and C-6 positions of the pyridinium core.[25] Clearly, the tilt of intervening aryl rings with respect to the plane of the pyridinium center (Chart 1) contributes to weakening the efficiency of the propagation of mesomeric electronic effects. The direct substitution of pyridinium centers[6,7] therefore appears desirable as the only way to strongly modify their electrochemical features and reach the targeted range of reduction potentials.[26]

2. Molecular Design

Pyridinium is actually in itself a choice influential group to improve the electron-accepting ability of pyridinium electrophores,[7,16] as demonstrated by the benchmark electrochemical behavior of viologens,[27] namely, 1,1′-dialkyl-4,4′-bipyridiniums ("paraquats"; Chart 2b),[28] 1,1′-dialkyl-2,2′-bipyridiniums ("diquats"), and other dimeric combinations.[29] From the analysis of the features of the LUMO of reference *N*-methylpyridinium (see Figure S-55, Supporting Information), one can derive the most relevant connection scheme to optimize the mutual influences of two directly linked pyridiniums. Constraints related to forthcoming uses of the new EPs, that is, stability (chemical, thermal, and photochemical), must also be taken into account as well as their possible well-defined attaching to other functional subunits. Sorted by decreasing order of magnitude, atomic contributions to the LUMO are lying at positions C-4 > N-1 > C-2 and C-6 ≫ C-3 and C-5 (Chart 2a and Figure S-55, Supporting Information). This observation suggests that the most efficient interpyridinium connections should involve the following pairs of positions: C-4/C-4 (rank 1), C-4/N-1 (rank 2), and then N-1/N-1 (rank 3), given that the larger the associated coefficients, the greater the mutual influence. Chart 2 illustrates the interpyridinium connections above mentioned.

Chart 2. Most Efficient Inter-Pyridinium Connections Discussed in the Text along with the Adopted Numbering Scheme for the Pyridinium Entity: C-4/C-4 (b), C-4/N-1 (c), and N-1/N-1 (d)[a]

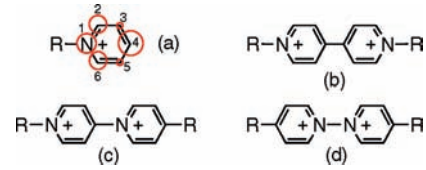

[a] Red circles are pictorial representations of atomic contributions to the LUMO (absolute values) of the *N*-methylpyridinium.

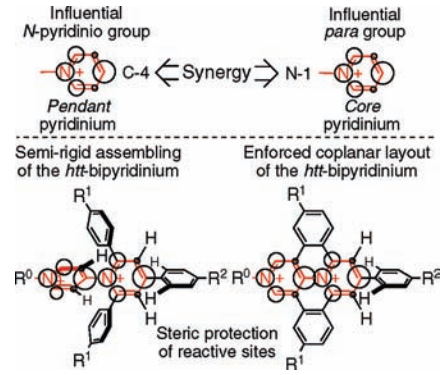

Figure 1. Key elements of the molecular design. Circles are pictorial representations of atomic contributions to the LUMO (absolute values) of the pyridinium building block.

However, due to the very similar contributions of atomic orbitals of the C-4 and N-1 atoms to the LUMO, the efficiencies of the first two pairs are comparable. The C-4/N-1 configuration is dissymmetric, which permits one to distinguish the functions of the two pyridiniums (Figure 1). Here, the pyridinium engaging the lower coefficient (i.e., N-1) can be formally considered as the substituent of the other pyridinium at the C-4 position. The former is hereafter referred to as the core

(25) Typical nitro substitutions of tetrabranched pyridinium (**TP** in Chart 1) give the following values for the first reduction potential (vs SCE in MeCN):−0.70 (with R1 = H and R2 = NO_2) and−0.65 V (with R1 = NO_2 and R1 = H); see ref 24b.

(26) As an illustration of the effect of direct substitution, one can cite the case of *N*-(2-pyrimidyl)pyridinium derivatives, which are reversibly one-electron reduced at ca.−0.36 V vs SCE in MeCN, see: (a) Coe, B. J.; Beyer, T.; Jeffery, J. C.; Coles, S. J.; Gelbrich, T.; Hursthouse, M. B.; Light, M. E. *J. Chem. Soc., Dalton Trans.* **2000**, 797–803. (b) Coe, B. J.; Harris, J. A.; Jones, L. A.; Brunschwig, B. S.; Song, K.; Clays, K.; Garin, J.; Orduna, J.; Coles, S. J.; Hursthouse, M. B. *J. Am. Chem. Soc.* **2005**, *127*, 4845–4859. (c) Coe, B. J.; Harris, J. A.; Brunschwig, B. S.; Asselberghs, I.; Clays, K.; Garin, J.; Orduna, J. *J. Am. Chem. Soc.* **2005**, *127*, 13399–13410.

(27) Michaelis, L. *Biochem. Z.* **1932**, *250*, 564–567.

(28) The first reduction process related to pyridinium occurs at a potential value that is typically shifted from ca.−1.30 to ca.−0.44 V (vs SCE in MeCN) on going from the *N*-methylpyridinium monomer to the *N*-methylviologen (**MV**) dimer (i.e., "paraquat").

(29) Wardman, P. *J. Phys. Chem. Ref. Data* **1989**, *18*, 1637–1755, and references therein.

Chart 3. Molecular Structures along with Related Labels of the Branched and Fused EPs Studied, Including Three Reference EPs (**Rf** (this work), **RfB**,[16] and **RfF**[16]) and Two Additional Pyridinium-Based References (i.e., methylviologen, **MV**, and 2,7-dimethyl-diazapyrenium, **DMDAP**)[a]

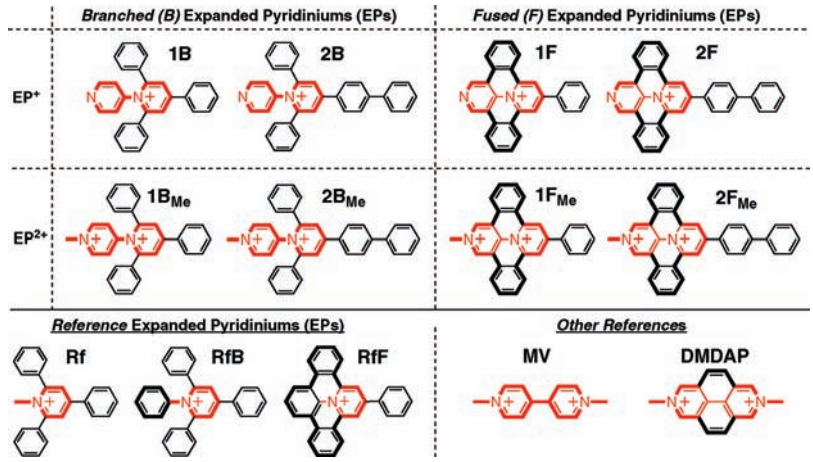

[a] Counteranions are BF_4^- for monocationic expanded pyridiniums (EP^+) and PF_6^- for dicationic expanded *htt*-bipyridiniums (EP^{2+}).

Table 1. Reduction Data of the Studied Compounds and Some Reference Species (vs SCE) at Pt Electrode for Acetonitrile Solutions (+0.1 M NBu_4PF_6) at Room Temperature[a]

entry	$E_{1/2}$, V (ΔE_p, mV)	*n*	$E_{1/2}$, V (ΔE_p, mV)	*n*
Rf	−1.07 (90)	1	−1.53 (97)	1
RfB[b]	−1.00 (77)	1	−1.16 (96)	1
1B	−0.93 (115)	2		
2B	−0.91 (115)	2		
1B$_{Me}$	−0.60 (102)	2		
2B$_{Me}$	−0.58 (102)	2		
RfF[b]	−1.00 (117)	1	−1.77 (102)	1
1F	−0.84 (114)	1	−1.61 (83)	1
2F	−0.83[c]	1	−1.57[c]	1
1F$_{Me}$	−0.43 (88)	1	−1.08 (198)	1
2F$_{Me}$	−0.42 (85)	1	−1.07 (213)	1
MV[d]	−0.44 (84)	1	−0.86 (86)	1
DMDAP[e]	−0.44[e]	1	− 0.93 (irr.)[e]	1
NI/PI [f]	−0.48/−0.43	1	− 0.99/−0.70	1
C_{60}[g]	−0.44	1	−0.82	1
BQ[h]	−0.47	1		

[a] Unless otherwise noted, $E_{1/2}$ (vs SCE) is calculated as $(E_{pa} + E_{pc})/2$, where E_{pa} and E_{pc} are the anodic and cathodic peak potentials measured by cyclic voltammetry at 0.1 V s^{-1}, ΔE_p is the difference of potential between E_{pc} and E_{pa}, *n* is the number of electrons involved in the redox process determined by rotating disk electrode voltammetry by comparison with reference components or with respect to an internal monoelectronic oxidation of ferrocene (see text below about EP-based dyads). For more details, see the Experimental Section. [b] From ref 16. [c] From square-wave measurement. [d] **MV**, see Chart 3; data determined in this work; see also ref 33. [e] **DMDAP**; see Chart 3; data from ref 34; irr., irreversible process; these reduction potential values should be compared with those of **MV** measured in the same conditions, i.e., −0.40 and −0.82 V, see ref 34. [f] **NI** is naphthalene-tetracarboxydiimide, and **PI** is perylene-tetracarboxydiimide; measured in DMF; see ref 35. [g] Measured in CH_2Cl_2 vs SCE, from ref 36. [h] **BQ** is benzoquinone; see ref 37.

pyridinium, while the latter is identified as the pendant pyridinium (Figure 1). This functional distinction is tightly bound to the notion of gradient and is of utmost interest when dealing with vectorial electron and/or energy transfers or transports. Thus, the (C-4/N-1) "head-to-tail" (*htt*) manner to assemble pyridiniums deserves to be assessed as a promising alternative to the symmetric (C-4/C-4) "tail-to-tail" dimerization embodied in popular viologens (Chart 2).

To ensure the chemical and electrochemical stability of pyridiniums vis-à-vis nucleophilic attacks (including reductive dimerization or pimerization) at the C-4 position of both the pendant and the core pyridiniums, aryl groups are appended at either side of the core $N_{pyridinio}$ atom (thereby also protecting the interpyridinium linkage)[30] and para to it,[31] respectively (Figure 1). Branched EPs made up of two redox sites forming the *htt*-bipyridinium subsystem are anticipated to efficiently manage with two electrons, as is the case for viologens. However, this will be done differently due to intramolecular steric hindrance and/or the central position of the core $N_{pyridinio}$ atom. The pyridinium-localized nature of the LUMO can be turned to good account by embedding the *htt*-bipyridinium redox-active subsystem within the planar molecular scaffold of fused polycyclic EPs, which allows for locking the two heteroaromatic fragments in a coplanar conformation, hence optimizing their synergistic interaction. At the same time, pericondensation is also likely to favorably impact the electronic and photophysical properties. Lastly, it is worth noting that substituents R^2, primarily, and to a lesser extent R^1 and R^0, can be replaced with functional subunits to build multicomponent architectures.

Here we report the syntheses, redox behavior, electro-optical features, and luminescence properties of eight expanded pyridiniums featuring a "head-to-tail" (*htt*) topology. This investigation was conducted both experimentally and theoretically. The compounds studied are shown in Chart 3. In our nomenclature, **1** identifies species that have a single phenyl at the C-4 position of the pyridinium core, whereas species of the **2** series bear a C-4 biphenyl group; moreover, **B** stays for branched compounds, while **F** indicates fused ones (see Chart 3); finally, the **Me** subscript indicates *N*-methylated species. It can be noted that dicationic compounds **1B$_{Me}$**, **2B$_{Me}$**, **1F$_{Me}$**, and **2F$_{Me}$** are derived from **1B**, **2B**, **1F**, and **2F**, respectively,[32] by the quaternarization

(30) (a) Katritzky, A. R.; Marson, C. *Angew. Chem., Int. Ed. Engl.* **1984**, *23*, 420–429. (b) Katritzky, A. R. *Tetrahedron* **1980**, *36*, 679–699.
(31) Volke, J.; Dunsch, L.; Volkeova, V.; Petr, A.; Urban, J. *Electrochim. Acta* **1997**, *42*, 1771–1780.
(32) **1B**, 2,4,6-triphenyl-1,4′-bipyridin-1-ium; **1B$_{Me}$**, 1′-methyl-2,4,6-triphenyl-1,4′-bipyridine-1,1′-diium; **2B**, 4-(biphenyl-4-yl)-2,6-diphenyl-1,4′-bipyridin-1-ium; **2B$_{Me}$**, 4-(biphenyl-4-yl)-1′-methyl-2,6-diphenyl-1,4′-bipyridine-1,1′-diium; **1F**, 9-phenyl-benzo[*c*]benzo[1,2]quinolizino[3,4,5,6-*ija*][1,6]naphthyridin-15-ium; **1F$_{Me}$**, 2-methyl-9-phenyl-benzo[*c*]benzo-[1,2]quinolizino[3,4,5,6-*ija*][1,6]naphthyridin-2,15-diium; **2F**, 9-(biphenyl-4-yl)-benzo[*c*]benzo[1,2]quinolizino[3,4,5,6-*ija*][1,6]naphthyridin-15-ium; **2F$_{Me}$**, 9-(biphenyl-4-yl)-2-methyl-benzo[*c*]benzo[1,2]quinolizino[3,4,5,6-*ija*][1,6]naphthyridin-2,15-diium.

of the nitrogen atom of their pendant pyridine moiety, whereas **1F**, **2F**, $\mathbf{1F_{Me}}$, and $\mathbf{2F_{Me}}$ are the fused analogues of **1B**, **2B**, $\mathbf{1B_{Me}}$, and $\mathbf{2B_{Me}}$ branched species, respectively.

3. Results and Discussion

3.1. Expanded Bipyridiniums as Electrophores: Reduction Behavior. The investigated species undergo reversible reduction processes at mild potentials. Table 1 shows the data of the studied EPs (see also Supporting Information) together with relevant data of reference species and other well-known electron acceptors.

As expected, the first reduction potential moves to less negative values (anodic shift) when passing from monocharged pyridiniums (EP^+) to quaternarized, dicharged, bipyridinium species (EP^{2+}) by ca. +370 mV on average (Table 1 and Figure 2). The impact of pericondensation is comparatively smaller in absolute values: ca. +85 and +165 mV on average for monocationic (**1B**/**1F** and **2B**/**2F**) and dicationic ($\mathbf{1B_{Me}}$/$\mathbf{1F_{Me}}$ and $\mathbf{2B_{Me}}$/$\mathbf{2F_{Me}}$) species, respectively. Comparison with other commonly used and well-known systems as electron-acceptor species (see Table 1) indicates that the studied compounds are fairly good electron acceptors since the quaternarized species $\mathbf{2B_{Me}}$, $\mathbf{1B_{Me}}$, $\mathbf{2F_{Me}}$, and $\mathbf{1F_{Me}}$ have redox properties similar to those of the best electron-acceptor systems.

The bielectronic nature of the first reduction process of the four branched species (**1B**/**2B**−$\mathbf{1B_{Me}}$/$\mathbf{2B_{Me}}$) is a very interesting result (Table 1). This electrochemical feature is unambiguously demonstrated by performing rotating disk electrode voltammetry on purposely synthesized ferrocenyl-substituted EPs, namely, **2B**-Fc and **2F**-Fc dyads (Figure 3). The well-established one-electron oxidation attached to the ferrocene (Fc) subunit serves as internal reference to determine the number of electron(s) involved in the reduction processes of the EP parts of these dyads (Figure 3).

Roughly, bielectronic processes usually occur when (i) two identical and noninteracting (at least from the electrostatic viewpoint) redox sites are present in the same (super)molecule and (ii) when adding/removing a second electron is easier than adding/removing the first one; the latter phenomenon, known as "potential inversion", is usually associated to structural changes[38] or gains in "electronic stability" (e.g., aromaticity).[21] In the present case, the bielectronic reduction is most likely due to a "potential inversion" phenomenon attached to a huge structural change upon reduction. Typically, a change in the hybridization of the $N_{pyridinio}$ atom of the pyridinium core, accompanied by its pyramidalization, is hypothesized. Such a redox-triggered pyramidalization has been recently computed in the two following cases: (1) the two-electron-reduced hexaaryl-substituted pyridinium[16] (**XP** in Chart 1) and (2) the relaxed singlet excited charge-transfer state of pyridinium-*N*-phenolate betaine B30.[39] In the case of tetrabranched EPs, this redox-triggered reorganization of the molecular structure is assumed to be fluxional in nature, hence the observed electrochemical reversibility. The characterization of this dynamic distortion is currently underway.

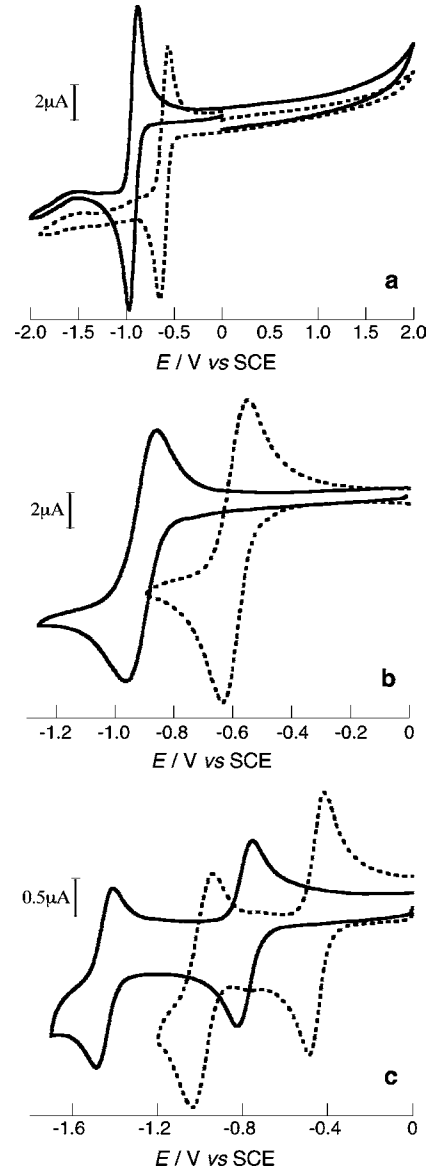

Figure 2. Illustration of the impact of quaternarization: EP^+ (solid) and EP^{2+} (dotted). Cyclic voltammograms: (a) **1B** ($c = 6 \times 10^{-4}$ M) and $\mathbf{1B_{Me}}$ ($c = 5 \times 10^{-4}$ M), (b) **2B** ($c = 5.5 \times 10^{-4}$ M) and $\mathbf{2B_{Me}}$ ($c = 6 \times 10^{-4}$ M), and (c) **2F** ($c = 3 \times 10^{-4}$ M) and $\mathbf{2F_{Me}}$ ($c = 6 \times 10^{-4}$ M) in MeCN (a, b) or DMSO (c) + 0.1 M $TBAPF_6$ (Pt electrode, $v = 100$ mV s^{-1}).

With respect to branched EPs, even though the first two monoelectronic reductions are merged into an apparent bielectronic process when experimentally investigated, it is worth clarifying the identity of the actual site of the first reduction in view of the possible use of these compounds as electron-acceptor components within polyad assemblies.[23,24] Theory shows that the first electron added to the molecule is essentially located on the pyridinium core within species **1B** and **2B**, whereas it is delocalized over both pyridinium fragments within $\mathbf{1B_{Me}}$ and $\mathbf{2B_{Me}}$, with the pendant one adopting the characteristic quinoïdal

(33) Takahashi, K.; Nihira, T.; Akiyama, K.; Ikegami, Y.; Fukuyo, E. *J. Chem. Soc., Chem. Commun.* **1992**, 620–622.
(34) Hünig, S.; Gross, J. *Tetrahedron Lett.* **1968**, *21*, 2599–2604. 1968, *21*, 4139.
(35) Gosztola, D.; Niemczyk, M. P.; Svec, W.; Lukas, A. S.; Wasielewski, M. R. *J. Phys. Chem. A* **2000**, *104*, 6545–6551.
(36) Dubois, D.; Kadish, K. M.; Flanagan, S.; Haufler, R. E.; Chibante, L. P. F.; Wilson, L. J. *J. Am. Chem. Soc.* **1991**, *113*, 4364–4366.
(37) Frontana, C.; Vazquez-Mayagoitia, A.; Garza, J.; Vargas, R.; Gonzalez, I. *J. Phys. Chem. A* **2006**, *110*, 9411–9419.
(38) (a) Evans, D. H.; Hu, K. *J. Chem. Soc., Faraday Trans.* **1996**, *92*, 3983–3990. (b) Evans, D. H. *Chem. Rev.* **2008**, *108*, 2113–2144.
(39) Catalan, J.; Garcia de Paz, J. L.; Reichardt, C. *J. Phys. Chem. A* **2010**, *114*, 6226–6234.

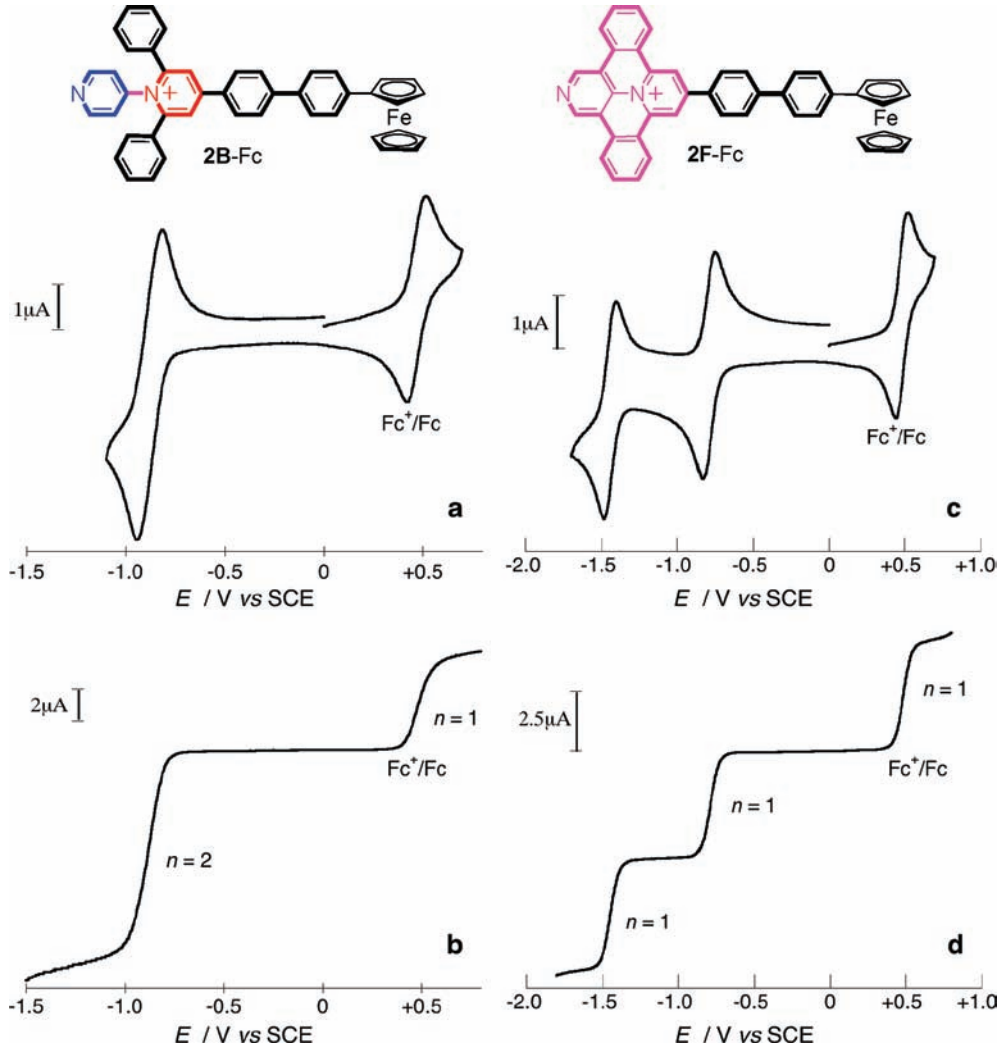

Figure 3. Determination of the number of electrons (n) involved in the first reduction processes of branched and fused pyridiniums, and assessment of electrochemical reversibility. (Left) Dyad **2B**-Fc ($c = 3.0 \times 10^{-4}$ M in MeCN): (a) cyclic voltammetry ($\upsilon = 0.1$ V s^{-1}) and (b) rotating disk electrode voltammetry ($\upsilon = 0.01$ V s^{-1}; rotation rate: $= 2 \times 10^3$ rpm). (Right) Dyad **2F**-Fc ($c = 6.0 \times 10^{-4}$ M in DMSO): (c) cyclic voltammetry ($\upsilon = 0.1$ V s^{-1}) and (d) rotating disk electrode voltammetry ($\upsilon = 0.01$ V s^{-1}; rotation rate $= 2 \times 10^3$ rpm).

pattern for reduced pyridinium, as expected (Figure 4). This result is straightforwardly explained by the well-established critical contribution to the LUMO of the carbon atom at position 4 of pyridinium rings (see Figure S-55, Supporting Information). For monocationic EPs, the core pyridinium bears a phenyl or biphenyl group at this pivotal site (Chart 3), whereas for dicationic branched EPs, which comprise two pyridinium motives, the pendant one bears the electron-withdrawing pyridinium core as the 4-substituent, hence its greater electron-accepting strength (Figure 1). The same holds for pericondensed species, including with regard to the fully developed quinoidal signature attached to the peripheral (pendant) *N*-pyridinium (see Figure 4). Interestingly, the reduction site remains localized on the pyridinium motives regardless of the degree of extension of the π-conjugated systems (branched or fused). This is in accordance with our previous findings derived from the comparative study of EPs based on a, single, pyridinium core (Chart 1).[16,17]

Last, the observation that the first reduction process occurs at less negative potentials within fused EPs than in their branched analogues remains to be commented on: −0.93 V for **1B** versus −0.84 V for **1F** and −0.60 V for $\mathbf{1B_{Me}}$ versus −0.43 V for $\mathbf{1F_{Me}}$ for representative instances (Table 1). The above-established relevance of the localized description of the electrochemical properties points to the enforced coplanar layout of the two heteroaromatic fragments within fused molecular scaffolds as the most likely explanation of these potential variations (rather than a hypothetical lowering of the energy of the LUMO upon extending the π-conjugated systems). Similar impacts of the change of the interannular angle on the redox properties of bipyridinium, namely, the anodic shift of the first reduction potential upon decreasing this twist angle, have already been reported in the literature.[6,40] This issue is further substantiated by the observation that the first reduction potential of both methylviologen (**MV**) and affiliated planar diazapyrenium (**DMDAP**; see Chart 3) amount to very close values (within 0.04 V; see Table 1), bearing in mind that pyridinium rings are not far from coplanarity within **MV**.

(40) (a) Benniston, A. C.; Harriman, A.; Li, P.; Rostron, J. P.; Harrington, R. W.; Clegg, W. *Chem.—Eur. J.* **2007**, *13*, 7838–7851. (b) Beer, P. D.; Chen, Z.; Grieve, A.; Haggitt, J. *J. Chem. Soc., Chem. Commun.* **1994**, 2413–2414. (c) Kodaka, M.; Kubota, Y. *J. Chem. Soc., Perkin Trans.* **1999**, *2*, 891–894. (d) Willner, I.; Ayalon, A.; Rabinovitz, M. *New J. Chem.* **1990**, *14*, 685–688. (e) Chen, P.; Curry, M.; Meyer, T. J. *Inorg. Chem.* **1989**, *28*, 2271–2280. (d) Thummel, R. P.; Lefoulon, F.; Chirayil, S.; Goulle, V. *J. Org. Chem.* **1988**, *53*, 4745–4747.

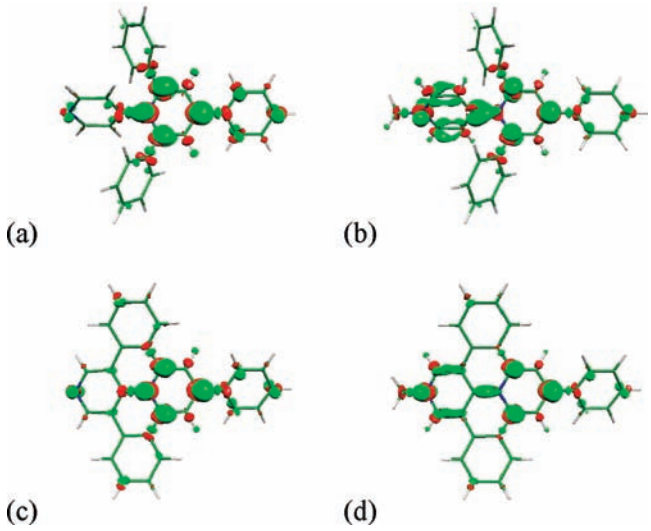

Figure 4. Illustration of the expansion of the site of first reduction upon quaternarization (*N*-alkylation). Difference in total density computed between the monoreduced and native forms (at the geometry of the reduced species, isocontour = 0.0025 au) of **1B** (a), $\mathbf{1B_{Me}}$ (b), **1F** (c), and $\mathbf{1F_{Me}}$ (d). Green lobes indicate an increase of total electron density (red lobes indicate a depletion).

3.2. Expanded Bipyridiniums as Chromophores: Absorption Spectra. The absorption spectra of branched compounds $\mathbf{1B}/\mathbf{2B}-\mathbf{1B_{Me}}/\mathbf{2B_{Me}}$ (Figure 5 and Table S-1, Supporting Information) exhibit an intense band in the 280−440 nm region. This can be assigned to the lowest energy spin-allowed $\pi-\pi^*$ transitions on the basis of molar absorption coefficients and band shapes. The absorption spectrum of reference **Rf** (lacking the *N*-pyridinio aryl group; see Chart 3) closely resembles that of **1B**. This is not surprising since TD-DFT calculations tell us that the electronic transitions present in this spectral region essentially originate from intramolecular charge transfers (ICT) involving electron-releasing aryl substituents at positions 2, 6, and 4 only, on the one hand, and the electron-withdrawing pyridinium core, on the other (see Supporting Information).[41] The main band is red shifted on passing from **1B** and $\mathbf{1B_{Me}}$ to **2B** and $\mathbf{2B_{Me}}$, respectively, when a biphenyl subunit is present. This observation suggests, in agreement with theoretical calculations (see TD-DFT outcomes in Supporting Information), that for the species that contain a biphenyl substituent the ICT character is further enhanced. The biphenyl fragment is a better electron-releasing group than a mere phenyl, thereby raising accordingly the energy of the HOMO. The absorption band is red shifted on moving from the monopyridiniums (**1B** and **2B**) to the bipyridiniums ($\mathbf{1B_{Me}}$ and $\mathbf{2B_{Me}}$). This not only agrees with the above ICT hypothesis but also indicates that electron-acceptor moieties present in the latter EPs are significantly stronger than in the former, in accordance with redox properties (see Table 1).

The fused species (**F** series) exhibit much more complex absorption spectra than their corresponding branched counterparts (Figure 5, Table S-1, Supporting Information). The spectra are more structured and red shifted, and apparently more transitions contribute to the absorption features. Structured bands may be justified if fused species are considered to exhibit more rigid structures than the corresponding branched pyridiniums. In such a case, the nuclear configurations of ground and excited states are more similar, and therefore, radiative transitions between these states yield structured spectra (including for absorption). Moreover, a pronounced vibronic effect ascribable to the coupling of the ICT transition that involves the dangling (bi)phenyl terminus and its torsional motion[15−17] also contributes to the absorption features. This effect is clearly visualized at the red edge of the absorption spectra of **1F** and $\mathbf{1F_{Me}}$ (Figures 5 and 6).

Upon pericondensation, a densification of MOs close to the HOMO−LUMO gap was computed and revealed the increasing complexity of the absorption spectra when going from branched to fused chromophores (Figure 6). In parallel, there occurred two concomitant phenomena that explain the observed reduction of the HOMO−LUMO gap. On the one hand, the LUMOs are computed to lie at lower energy in the fused species than in the corresponding branched EPs. This finding is in agreement with the evolution of the first reduction potentials experimentally measured (e.g., compare the first reduction potential of **2B**, −0.91 V, with that of **2F**, −0.83 V, or the first reduction potential of $\mathbf{2B_{Me}}$, −0.58 V, with that of $\mathbf{2F_{Me}}$, −0.42 V; see Table 1). This variation has been ascribed to different values for the critical twist angle between the pyridinium core and its *N*-pyridyl(ium) influential fragment, that is, differential electronic delocalization within (i.e., intra) *htt*-bipyridin(ium) subsystems (see above). On the other hand, the computed energies of the HOMOs are higher for the fused EPs than for the corresponding branched ones, which is a direct electronic consequence of pericondensation.[16] As a result, the HOMO−LUMO gaps of the fused systems are smaller than those of the corresponding branched EPs, thereby explaining the observed

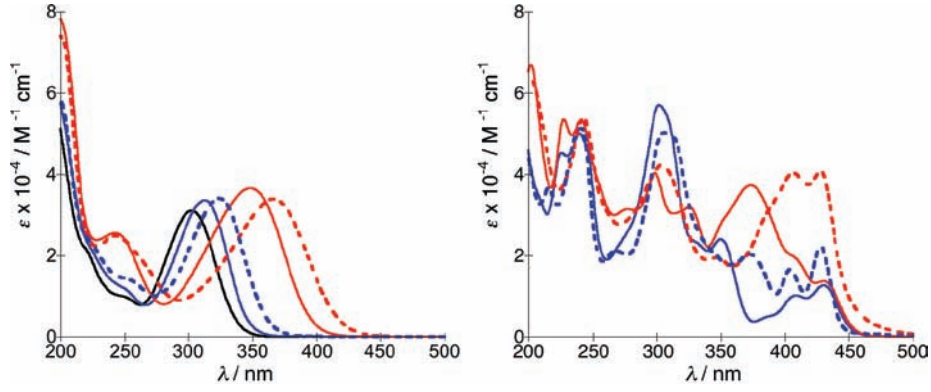

Figure 5. Electronic spectra of branched (left) and fused (right) derivatives (acetonitrile solutions). (Left) Solid blue line, **1B**; dashed blue line, $\mathbf{1B_{Me}}$; solid red line, **2B**; dashed red line, $\mathbf{2B_{Me}}$; black line, **Rf**. (Right) Solid blue line, **1F**; dashed blue line, $\mathbf{1F_{Me}}$; solid red line, **2F**; dashed red line, $\mathbf{2F_{Me}}$. For related data, see Table S-1 in the Supporting Information.

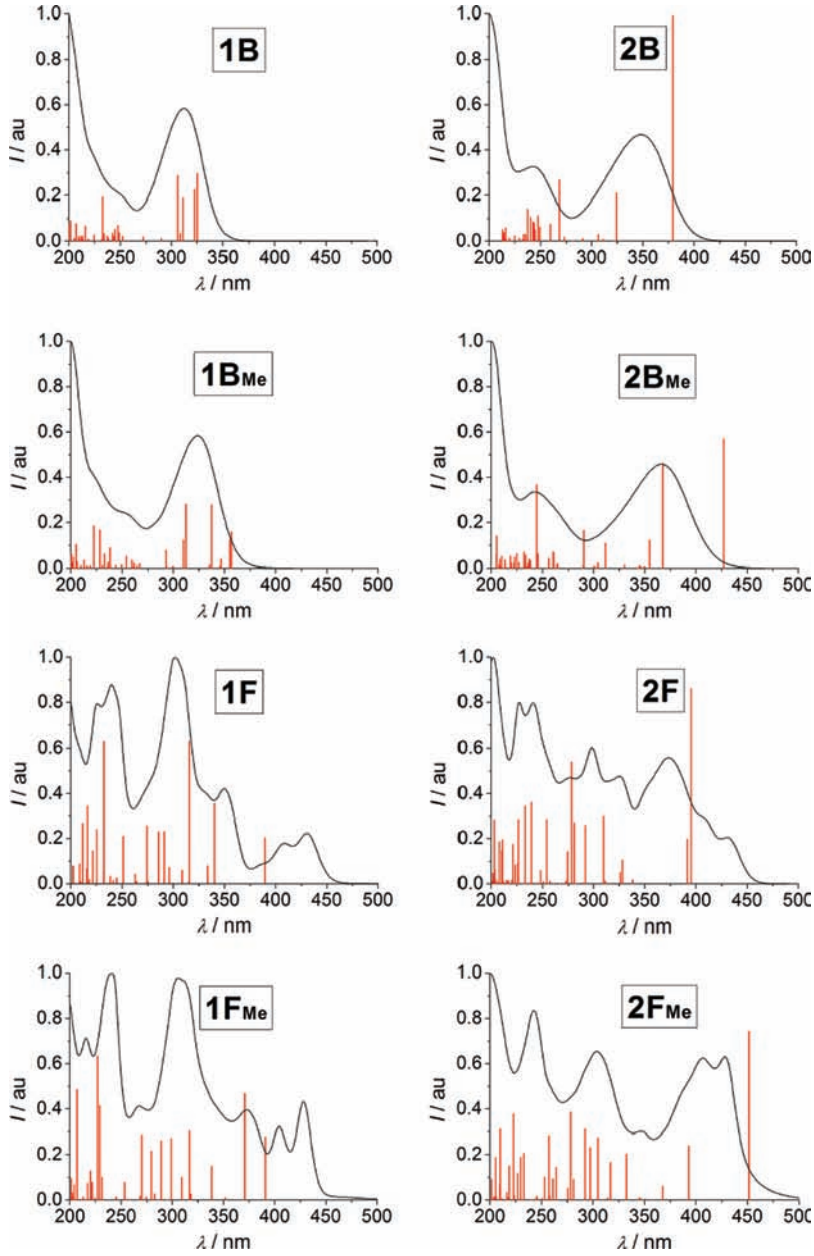

Figure 6. Superimposed experimental absorption spectra and calculated electronic transitions.[42]

red-shifted absorption on moving from **1B**/**2B** and $\mathbf{1B_{Me}}$/$\mathbf{2B_{Me}}$ to **1F**/**2F** and $\mathbf{1F_{Me}}$/$\mathbf{2F_{Me}}$.

It is also interesting to note that the presence of the biphenyl subunit in **2F** and $\mathbf{2F_{Me}}$ does not translate into a clear red shift of the lowest-energy band for the fused systems, conversely to branched analogues (Figure 5 and Table S-1, Supporting Information). Indeed, inspection of the MO involved in the first electronic transition in the case of both **2F** and $\mathbf{2F_{Me}}$ confirms its ICT character from a HOMO (essentially localized on the biphenyl substituent) to a LUMO centered on the core pyridinium (**2F**) (Supporting Information) or pendant pyridinium ($\mathbf{2F_{Me}}$) (Figure 7). The ICT character correctly translates in an increase of intensity associated to the first band experimentally observed when going from **1F** and $\mathbf{1F_{Me}}$ to **2F** and $\mathbf{2F_{Me}}$. Nevertheless, since the HOMO of **2F** and $\mathbf{2F_{Me}}$ (localized on the biphenyl) is computed to be very close in energy to the HOMO−1 (π orbital localized on the fused scaffold and identical to the HOMO of the corresponding **1F** and $\mathbf{1F_{Me}}$

(41) Similar assignment also holds for analogous 1*N*,2,4,6-tetraarylpyridiniums bearing a (substituted) phenyl group at the 1*N* position instead of the pyridyl fragment; see ref 14 and also: (a) Kharlanov, V. A.; Knyazhansky, M. I. *J. Photochem. Photobiol. A* **1999**, *125*, 21–27. (b) Knyazhansky, M. I.; Kharlanov, V. A.; Tymiansky, Ya. R. *J. Photochem. Photobiol. A* **1998**, *118*, 151–156.

(42) In this context it is worth reminding that the intensity (/energy) of the computed CT transition can be slightly overestimated (/underestimated) when using a TD-DFT approach even in conjunction with a hybrid functional (such as in the present case), see, for instance: (a) Jacquemin, D.; Perpete, E. A.; Ciofini, I.; Adamo, C. *Acc. Chem. Res.* **2009**, *42*, 326–334. (b) Dreuw, A.; Head-Gordon, M. *J. Am. Chem. Soc.* **2004**, *126*, 4007–4016. This effect is amplified and can yield completely unphysical results when the overlap between the orbitals involved in the excitation is small or nonexistent, as is the case for through-space CT. In the case of the chromophores studied here, a sizable overlap is present for all ICT considered. Thus, only a modest overestimation of oscillator strength associated with a slight shift in energy is expected for these transitions. This is indeed observed in the sensitive instances of **2B**, $\mathbf{2B_{Me}}$, **2F**, and $\mathbf{2F_{Me}}$ (Figure 6).

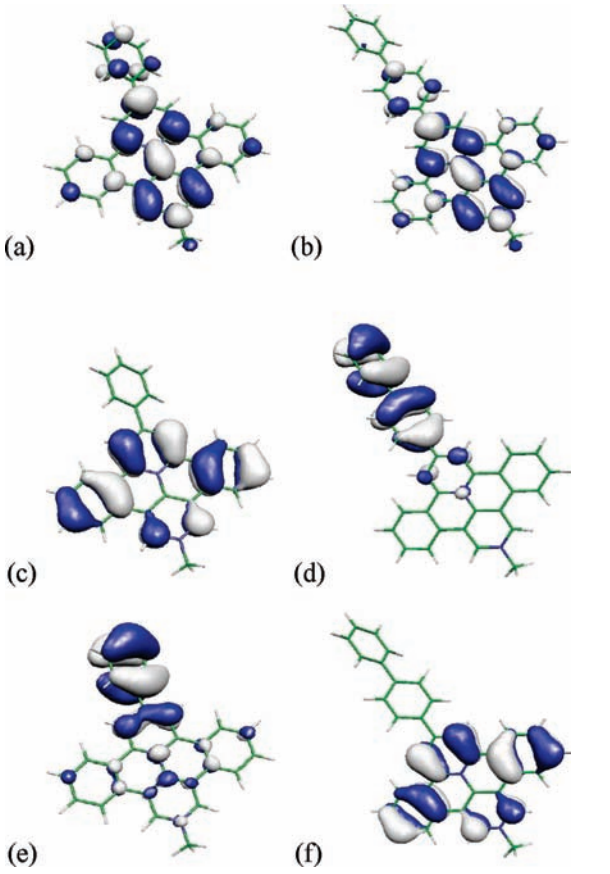

Figure 7. Frontier MOs of $\mathbf{1F_{Me}}$ and $\mathbf{2F_{Me}}$ (isocontour value = 0.025 au): (top) LUMO ($\mathbf{1F_{Me}}$ (a) and $\mathbf{2F_{Me}}$ (b)); (middle) HOMO ($\mathbf{1F_{Me}}$ (c) and $\mathbf{2F_{Me}}$ (d)); (bottom) HOMO−1 ($\mathbf{1F_{Me}}$ (e) and $\mathbf{2F_{Me}}$ (f)).[44]

compounds) the transition energies are not red shifted (Figures 6 and 7).[43,44]

To summarize, electro-optical features of branched EPs are essentially governed by ICT transitions, as illustrated by the steady bathochromic shift of their dominant large absorption band when going from the less polar chromophore (**1B**) to the most polar one: $\mathbf{2B_{Me}}$ (see Figure 5). Conversely, no such bathochromic shift of the red-edge absorption is observed for the series of fused analogues since frontier MOs are fortuitously near-degenerate and can therefore be interchanged on modifying the intramolecular ICT landscape without sizably impacting the HOMO−LUMO gap. Besides, absorptivity at the red edge is found to increase on enhancing the overall ICT character of the fused EPs due to additive contributions of vibronic effects and energy densification of electronic transitions. Overall, fused EPs have a smaller HOMO−LUMO gap than branched ones,

(43) In the case of molecule **2F**, the HOMO and HOMO−1 are near degenerate so that two very close transitions are computed. The first, very intense of ICT character is computed at 395 nm and the second, less intense corresponding to the HOMO−1 to LUMO excitation is computed at 391 nm. In such a case, it is not excluded that the two transitions could be inverted due to the underestimation of ICT energies at the TD-DFT level. From the comparison with the experimental absorption spectrum (Figure 6), this is apparently the case. In such a case it is not excluded, in agreement with the experimental data, that the emitting state could be the one corresponding to a HOMO−1 to LUMO excitation.

(44) For $\mathbf{1F_{Me}}$/$\mathbf{2F_{Me}}$, computed energies (au) of frontier MOs (Figure 7) are, respectively, the following: −0.137 (a)/−0.133 (b) for the LUMO; −0.278 (c)/−0.251 (d) for the HOMO, and −0.283 (e)/−0.275 (f) for the HOMO−1.

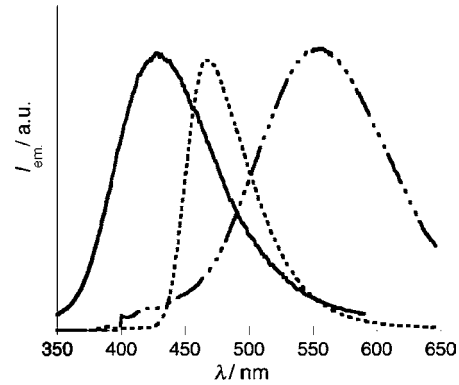

Figure 8. Luminescence spectra of **1B** (solid line), **2F** (dashed line), and $\mathbf{2B_{Me}}$ (dashed-dotted) in acetonitrile solution at room temperature.

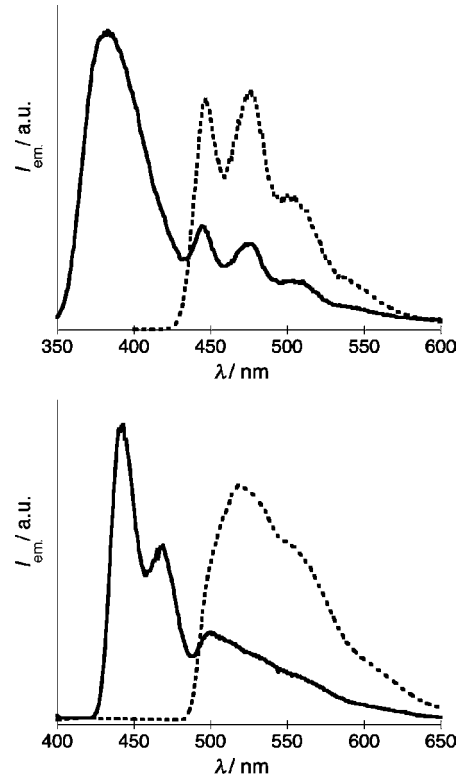

Figure 9. Luminescence spectra of **1B** (top) and **2F** (bottom) in MeOH/EtOH 4:1 (v/v) rigid matrix at 77 K. Dashed spectra (phosphorescence) are recorded by using a time delay of 10 ms from the excitation pulse.

which translates into a more extended absorption in the visible, and they exhibit more rich absorption spectra with larger integrated absorptivities.

3.3. Expanded Bipyridiniums as Luminophores: Emission Properties. All the compounds exhibit luminescence, both in fluid acetonitrile solutions at room temperature and in rigid matrices at 77 K in MeOH/EtOH 4:1 (v/v), with monoexponential decay in all cases. The luminescence data of the whole series of EP luminophores (Chart 3) along with relevant data of reference species including methylviologen (**MV**) and its diazapyrenium fused analogue (**DMDAP**) are collected in Tables 2 and 3; Figures 8 and 9 show representative emission spectra. In all cases, luminescence properties are independent of excitation wavelengths.

With regard to the room-temperature luminescence of branched EPs (**B** series), it is worth noting that the fluorescence quantum yields (Φ) of three of them (**2B**, $\mathbf{1B_{Me}}$, and $\mathbf{2B_{Me}}$) are in the

Table 2. Absorption (red edge) and Luminescence Data at Room Temperature in Acetonitrile

	absorption[a]	luminescence						
	λ, nm (ϵ, M^{-1} cm^{-1})	λ, nm	τ, ns	Φ	k_r, s^{-1}	k_{nr}, s^{-1}	$\Delta\nu$,[b] cm^{-1}	SS,[c] cm^{-1}
Rf	302 (31 000)	430	1.5	0.4	2.7×10^8	4.0×10^8	3900	9850
RfB[d]	308 (38 300)	480	3.0	$<10^{-4}$	$<3.3 \times 10^4$	$>3.3 \times 10^8$	4000	11 580
1B	312 (33 600)	435	0.2	0.04	2.5×10^8	6.0×10^9	3900	9060
2B	348 (36 600)	502	1.9	0.50	2.6×10^8	2.6×10^8	3950	8810
$\mathbf{1B_{Me}}$	323 (34 100)	455	0.4	0.22	5.5×10^8	1.9×10^9	4000	8880
$\mathbf{2B_{Me}}$	366 (33 900)	577	0.6	0.12	1.7×10^8	1.5×10^9	4170	9990
RfF[d]	429 (10 000)	465	7.0	0.35	5.0×10^7	9.3×10^7	3100	1800
1F	430 (12 700)	465	3.3	0.21	6.3×10^7	2.4×10^8	3000	1760
2F	430 (13 700)	480	3.1	0.21	6.8×10^7	2.5×10^8	2820	2430
$\mathbf{1F_{Me}}$	428 (22 200)	453	4.1	0.22	5.4×10^7	1.9×10^8	2150	1290
$\mathbf{2F_{Me}}$	428 (40 700)	610	2.8	0.10	3.6×10^7	3.2×10^8	3530	6970
MV[e]	260 (20 000)	353	0.9	0.02	2.2×10^7	1.1×10^9		10 130
DMDAP[e]	418 (15 000)	423	10.4	0.60	5.8×10^7	3.8×10^7		280

[a] The lowest-energy feature of the main absorption band is reported. [b] Half-width of the emission band. [c] Stokes shift, calculated as the difference in energy between the lowest-energy absorption feature and the emission maxima. [d] From ref 16. [e] From ref 19.

Table 3. Luminescence Data at 77 K in MeOH/EtOH 4:1 (v/v)

	fluorescence		phosphorescence	
	λ_{max}, nm	τ, ns	λ_{max}, nm	τ, ms
Rf	370	2.3	442	3240
1B	381	3.0	447	3000
2B	410	3.0	460	18
$\mathbf{1B_{Me}}$	407	1.5	453	700
$\mathbf{2B_{Me}}$	432	1.8	475	19
1F	441	5.3	506	800
2F	442	3.2	510	2000
$\mathbf{1F_{Me}}$	434	5.0	494	430
$\mathbf{2F_{Me}}$	430	3.5	540	175
MV[a]	330	7.0	418	3600
DMDAP[a]	424	10.7	586	900

[a] Recorded on butyronitrile rigid matrices; data from ref 19.

0.1−0.5 range (Table 2). This is close to the quantum yield of the reference **Rf** ($\Phi = 0.4$) and much greater than that of the loosely fluorescent *N*-phenyl-substituted **RfB** ($\Phi \approx 10^{-4}$).[16] The noticeable drop in photoluminescence quantum yield when going from **Rf** to **RfB** is ascribed to an intervening additional decay process due to an intramolecular charge-transfer state (ad-ICT) that involves the phenyl $N_{pyridinio}$ group as the donor (not present in **Rf**) and the pyridinium core as the acceptor, which promotes radiationless decay.[41,45] The dominant radiationless decay is an adiabatic structural relaxation toward coplanarity of the phenyl $N_{pyridinio}$ group with the pyridinium ring. Replacing the phenyl $N_{pyridinio}$ group with electron-withdrawing pyridine (case of **1B**) leads to an intermediate situation ($\Phi \approx 10^{-2}$), since it raises the energy of the above-mentioned ad-ICT state and thus approaches the photophysical behavior of reference **Rf**. Thus, one can reasonably ascribe the observed high emission quantum yields of the **B**-series species to (1) the mere suppression of the deleterious ad-ICT upon quaternarization of the pendant *N*-pyridyl group (cases of $\mathbf{1B_{Me}}$ and $\mathbf{2B_{Me}}$) or (2) the stabilization of the emitting ICT state by the presence of the better electron-releasing biphenyl. This stabilization rules out the higher-lying ad-ICT state that involves the pendant pyridine as the electron-releasing group and the pyridinium core as the acceptor (case of **2B**).

Concerning room-temperature photophysical properties as a function of the branched or fused nature of the EPs, a rough survey of the data of Table 2 indicates that the Stokes shift (SS) is quite different for the branched **B** species and for the fused **F** compounds. In fact, EPs of the **B** series exhibit quite large Stokes shifts, whereas the **F**-type species (with the partial exception of $\mathbf{2F_{Me}}$) exhibit much smaller ones. This is not surprising, when one considers that the excited state(s) of **B** compounds can undergo a significant structural reorganization process that leads to flattened relaxed geometries (*planarization* relaxation process).[17,24a,e] Another informative observation is the difference of broadness observed for the emission bands of the **B** and **F** series of EPs at room temperature (see values of half-height widths, $\Delta\nu$, in Table 2). Such values are larger for the branched **B** species, which confirms the larger distortion of the excited states of the branched species compared to the fused compounds. Indeed, adiabatic planarization is not an important relaxation process for **F** species since they have fused rigid and already largely planar overall molecular backbones.[46] In other words, the structures of branched and fused species are more similar at the excited state than at the ground state. Consequently, the excited state energy of analogous species (and as a consequence their luminescence spectra) tends to be similar, even if the absorption spectra look quite different. The above particularly applies to the **1B**/**1F** and $\mathbf{1B_{Me}}$/$\mathbf{1F_{Me}}$ couples of compounds. However, luminescence lifetimes are definitely shorter for **B**-type EPs than for **F**-type EPs, although emission quantum yields do not seem to follow a general trend on passing from the **B** to the **F** series (see Table 2). The k_r and k_{nr} radiative and nonradiative rate constants can be calculated from quantum yields and lifetime data (Table 2): both k_r and k_{nr} values are about 1 order of magnitude larger for the branched species compared to the fused compounds. The enhanced structure rigidity of the fused compounds can justify their smaller nonradiative decay rate constant, since some vibrations, which can assist the radiationless decay in the branched systems, are deactivated in the fused analogues. Moreover, the delocalized excitation over the whole π-conjugated system of fused poly-

(45) Knyazhansky, M. I.; Feigelman, V. M.; Tymyanski, Ya. R.; Druzhinin, S. I.; Uzhinov, B. M. *J. Lumin.* **1987**, *37*, 215–218.

(46) In agreement with the observed experimental trends, smaller Stokes shifts (Table S-2, Supporting Information) and structural rearrangements were computed in the case of fused systems with respect to the corresponding branched compounds, confirming the former's greater rigidity. More precisely, structural relaxation in both the singlet and the triplet excited states was computed to be mainly related to the planarization of the aryl substituents with respect to the central pyridinium core and proved to be larger in the case of nonfused architectures. For instance, the root mean square deviations (rmsd) computed between ground and singlet excited state structures for **1B** and **1F** are 0.23 and 0.11, respectively (and similar results hold for the other compounds).

cyclic EPs results in averaged distortions and reduced Franck−Condon factors.

It is also interesting to note that the EPs that comprise a biphenyl subunit (**2B**, **2B$_{Me}$**, **2F**, and **2F$_{Me}$**) show emission energies which are definitely red shifted compared to the emissions of the other species (Table 2). As for the absorption spectra of the branched chromophores, this observation suggests that the presence of the biphenyl group translates into a CT character of the excited state (and as a consequence of the emission) of the above-mentioned species. Comparing **2B** and **2B$_{Me}$** to the corresponding **1B** and **1B$_{Me}$**, this effect is not indicated by a larger Stokes shift, as is usually the case for CT emission, since for such compounds the lowest-energy absorption features already receive a significant CT contribution. On the contrary, for fused polycyclic luminophores that lack both the large photoinduced structural relaxation and the bathochromic shift of the absorption red edge usually associated with CT character (see section 3.2), the CT nature of the emission is clearly evidenced by the large Stokes shift. This is the case for **2F$_{Me}$** and, to a smaller extent, **2F**, as revealed by the comparison of their SS to those of their structural analogues **1F** and **1F$_{Me}$**, which exhibit an essentially "fused-core"-localized $\pi-\pi^*$ emission.[47]

As regards low-temperature photophysical properties, all compounds exhibit both fluorescence and phosphorescence at 77 K in MeOH/EtOH 4:1 (v/v) (see data in Table 3 and Figure 9). All emission spectra are structured (vibrational progression of about 1300 cm^{-1}, corresponding to C=C and C=N stretching) and can be assigned to locally excited $\pi-\pi^*$ singlet and triplet states. The absence of CT emission is justified if one considers that CT states with pronounced charge redistribution are largely destabilized in rigid matrix at low temperature, as a consequence of large nuclear barriers related to solvent reorganization.

The variations of the computed fluorescence and phosphorescence emission energies were also found in good qualitative agreement with experimental issues. While in the case of **1B**/**1B$_{Me}$** and **1F**/**1F$_{Me}$** (the **1**-type compounds) the $^1(\pi-\pi^*)$ S_1 excited state has an essentially "core-localized" character, calculations confirm the ICT character for the $^1(\pi-\pi^*)$ singlet excited state of all the systems that bear a biphenyl substituent (that is, **2B**/**2B$_{Me}$** and **2F**/**2F$_{Me}$**).

Let us now address the issue of the electronic features of structurally affiliated **MV** and **DMDAP** reference species (Tables 2 and 3) to complete the discussion of photophysical results. With regard to the impact of the extension of the π-conjugated system, it is worth noticing that the behavior of these two species parallel that of respective branched and fused EPs not only at the electrochemical level but also at both the electronic and photophysical levels. Typically, a scarce effect is detected for the first reduction process (see section 3.1), whereas absorption and emission properties are significantly different. More precisely, the electronic absorption spectrum is extended from the UV to the near visible (red-edge band at 418 nm) while becoming structured[19] on passing from **MV** to **DMDAP**. This is similar to trends observed when going from branched EPs (of type **1**) to their fused counterparts. Along the same line, **MV** is a poor luminophore at room temperature[19,48] whereas **DMDAP** is strongly fluorescent (its emission quantum yield amounts to 60%). These supplementary observations are also in line with our previous findings concerning EPs of the first generation (Chart 1)[16,17] and again confirm the relevance of the picture of pyridinium properties we put to the forth in our molecular design strategy (section 2). In the special case of pyridiniums, extending the π-conjugated system does not lower the energy of the LUMO accordingly (as reflected by the first reduction potentials). The LUMO remains localized on the pyridinium fragment(s), and electrochemistry fits a localized description, at least for the first reduction process. The situation is different for optical and photophysical properties. The sole features of the LUMO no longer govern them. Therefore, they fit a delocalized description and are sensitive to the degree of extension of the π-conjugated systems.

To summarize, branched and fused *htt*-EPs are equally good types of luminophores but, most important, are much better luminophores than parent bare pyridinium or bipyridinium species.

3.4. Insights into the Prerequisites of Photobiscyclization. Finally, on the basis of the insights we gained into the redox (section 3.1), electro-optical (section 3.2), and photophysical (section 3.3) behaviors of branched EPs, it is now possible to account, a posteriori, for the synthetic strategy empirically perfected to obtain the various fused EPs. This section is more specifically aimed at explaining observed differences in photochemical reactivity.

Indeed, fused EPs were obtained by the photochemical pericondensation of the proper branched EP precursors, following a route adapted from that described by Katritzky et al.[49] for the early synthesis of **1F**.[49a] Synthetic strategies are given in Scheme 1 (see also Supporting Information). These approaches were conceived because photobiscyclization pathways were found to be ineffective in the three following cases: (1) when the pendant *N*-pyridyl group is quaternarized (instance of **1B$_{Me}$**), (2) when a biphenyl group is appended at the C-4 position of the pyridinium core (instance of **2B**), and (3) when the branched EP is both quaternarized and derivatized with a biphenyl substituent (instance of **2B$_{Me}$**). Typical ^{1}H NMR spectra of the crude product of test photochemical reactions are given in the Supporting Information (see Figures S-34−S-37). The rationale of the relevant parameters that govern photoinduced cyclodehydrogenation is proposed below.

Photobiscyclization is known to take place from the singlet excited state of branched pyridiniums.[50] The maps of difference in total electron density between the relaxed lowest lying singlet excited state and the ground state (at the same geometry) were calculated for the four branched EPs (Figure 10 below) to account for this lack of photoreactivity. A comparative analysis of these maps enabled us to derive some qualitative criteria for photoinduced cyclodehydrogenation.

(47) However, whereas the luminescence data clearly indicate that the room temperature emissions of **2B**, **2B$_{Me}$**, and **2F$_{Me}$** are of CT nature, some doubt remains on the origin of the emission of **2F**. In fact, the Stokes shift of this compound, although larger than those of the analogues **1F** and **1F$_{Me}$**, is less pronounced compared to that of **2F$_{Me}$**, a bona fide CT emitter. For **2F**, on the sole basis of the experimental data, it is not possible to establish whether the $\pi-\pi^*$ emission essentially originates from a "fused-core" localized or an ICT transition or even exhibits a mixed character; see also ref 43.

(48) Peon, J.; Tan, X.; Hoerner, J. D.; Xia, C.; Luk, Y. F.; Kohler, B. *J. Phys. Chem. A* **2001**, *105*, 5768–5777.

(49) (a) Katritzky, A. R.; Zakaria, Z.; Lunt, E.; Jones, P. G.; Kennard, O. *J. Chem. Soc., Chem. Commun.* **1979**, 268–269. (b) Katritzky, A. R.; Zakaria, Z.; Lunt, E. *J. Chem. Soc., Perkin Trans.* **1980**, *1*, 1879–1887.

(50) Knyazhansky, M. I.; Metelitsa, A. V.; Makarova, N. I.; Feygelman, V. M.; Tymyansky, J. R. *J. Photochem. Photobiol. A* **2000**, *132*, 59–66.

Scheme 1. Synthetic Routes for the **1B**, **1B$_{Me}$**, **1F**, and **1F$_{Me}$** Series (left) as well as for the **2B**, **2B$_{Me}$**, **2F**, and **2F$_{Me}$** Series (right)[a]

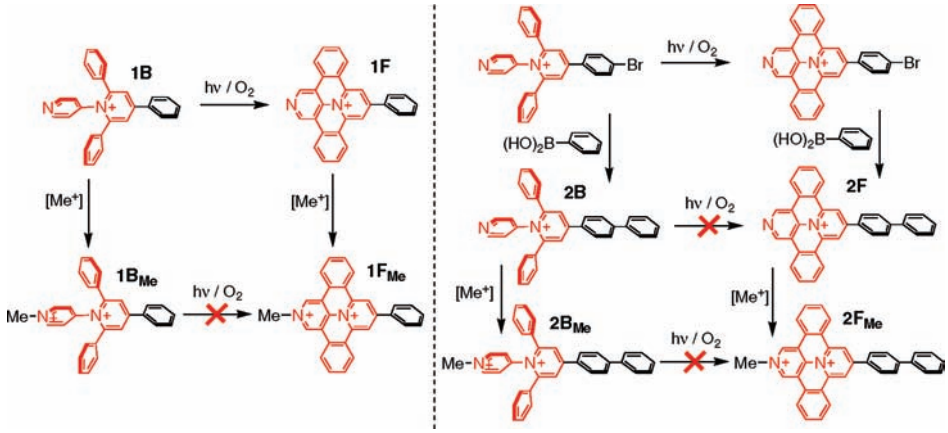

[a] [Me$^+$] is a methylating agent (see details in the Supporting Information).

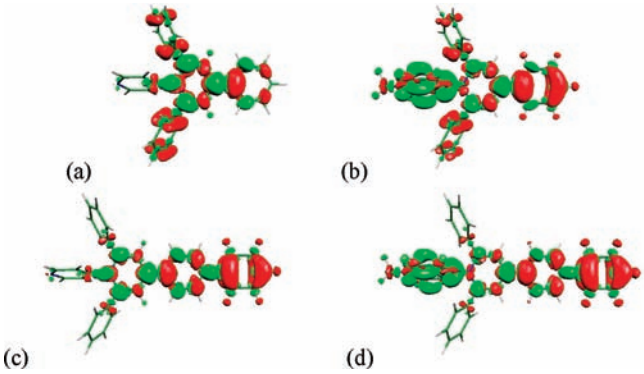

Figure 10. Electron-density difference maps of the lowest lying relaxed singlet excited state (S_1) as compared to the ground state (S_0) at the same geometry for **1B** (a), **1B$_{Me}$** (b), **2B** (c), and **2B$_{Me}$** (d); isocontour value = 0.001 au. The green (red) color indicates an increase (decrease) of electron density in a given molecular region upon excitation.

As can be seen in Figure 10 for the reference case of the photoconvertible **1B**, excited-state charge redistribution within ^{1}[**1B**]* corresponds to (i) an increase in electron density on the pyridinium core and its almost coplanar phenyl substituent at position 4 as well as on the four interannular linkages and (ii) the correlated significant decrease in electron density on the two phenyl branches ortho to the pyridinium nitrogen atom and, to a lesser extent, on the pyridyl *N*-group. Thereby, (i) the key planarization of the *N*-pyridinio group and of the two phenyl rings at positions 2 and 6 is induced (which is necessary to prepare subsequent pericyclic electron motion resulting in C−C bonds formation) and (ii) protons of electron-deficient aryls, which are destined to be abstracted during the rearomatization step with dioxygen (yielding to water molecules), are activated (Scheme 1). With regard to inhibition of photoinduced dehydrocyclization upon *N*-alkylation (reactivity loss of type 1, represented by the case of ^{1}[**1B$_{Me}$**]*), displaced electron density is no longer evenly redistributed around the central pyridinium but is almost entirely withdrawn by the pendant pyridinium. This situation is likely to favor the only planarization of the head-to-tail bipyridinium subsystem to the detriment of other phenyl substituents and in particular those connected at either side of the *N*-pyridinio group, hence preparing a conformation inappropriate to subsequent pericondensation. In addition, even if protons of phenyl 2,6-substituents of the pyridinium core are properly activated (weakening of C−H bonds upon electron-density depletion), those of the pendant pyridinium are, on the contrary, severely deactivated as a result of the reductive intramolecular charge transfer (ICT). Brought together, these two concomitant effects can explain the photostability of **1B$_{Me}$** (no trace of **1F$_{Me}$** was found in the ^{1}H NMR spectrum of the crude reaction product of the attempt of photobiscyclization; see Figure S-35 in the Supporting Information) versus the quantitative phototransformation observed in the cases of **1B** and **RfB** (see Figure S-34 in the Supporting Information).

With regard to the observed lack of photoreactivity for biphenyl derivatives (reactivity loss of type 2, represented by the case of ^{1}[**2B**]*), calculated electron density difference maps show that the photoactivated part of the molecule is not the one expected to be fused but instead the rodlike tricyclic molecular subsystem that encompasses the pyridinium core and the terminal biphenyl branch. In fact, if the relevant excited state is characterized by a pronounced ICT to the benefit of the pyridinium core, the activated protons are those of the electron-releasing phenyl terminus (decrease of electron density) rather than those of the targeted site of pericondensation. Consistently, a dramatic drop in the yield of photobiscyclization is expected, which was indeed found to be less than 5% for **2B** as judged from the ^{1}H NMR features of the crude photoreaction product of this branched EP (see Figure S-36, Supporting Information). All in all, the absence of photoinduced cyclodehydrogenation experimentally evidenced for the quaternarized EP which also bears a biphenyl branch as the 4-substituent, that is, **2B$_{Me}$** (reactivity loss of type 3), was therefore foreseeable (see Figure S-37, Supporting Information). As shown in Figure 10, a huge ICT takes place along the *htt*-bipyridinium main molecular axis, ultimately leading not only to the unsuitable activation of the protons of the electron-releasing phenyl terminus but also to the deleterious deactivation of the protons borne by the electron-withdrawing pendant pyridinium ring.

To summarize, we have shown here that experimental findings regarding the photochemical reactivity of branched expanded pyridiniums and more specifically their ability to undergo photobiscyclization into fused EPs can be correlated with maps corresponding to change in total electron density between the ground and the photoreactive $\pi-\pi^*$ singlet excited states. Qualitative criteria essentially relying on ICT features of these $^1(\pi-\pi^*)$ excited states could be derived, allowing forthcoming computer-assisted design of fused EP-based dyes, for instance. Manipulating the photoreactivity of branched EPs will rely on in-silico adjusting of the proper balance between various possible

ICT processes, which can be governed by peripheral substituents borne by the aryl branches of EPs.

4. Conclusion

In the present work we reported the design, synthesis, and characterization of the electronic, photophysical, and electrochemical properties of a series of novel expanded pyridiniums (EPs) featuring the so-called head-to-tail arrangement for their bipartite redox-active subsystem. We have shown that, regardless of their branched or fused nature, the most promising prototypes are the dicationic ones (quaternarized EPs), whether considering their chromophoric, luminophoric, or electrophoric behavior. Most importantly, on the basis of their performance appraisals, (i) large absorptivities ($\varepsilon > 10^4$ M^{-1} cm^{-1}) up to 450 nm, (ii) good luminescence quantum yields at room temperature ($\Phi_{Fluo} > 0.2$), and (iii) easily accessible first reduction potentials ($E_{red} \geq -0.6$ V vs SCE in MeCN), these EPs can be viewed as integrated multifunctional entities of interest in their own right. They could also serve as functional building blocks in various types of (supra)molecular devices, following the example of benchmark perylene bisimides.[51] Herein the described expanded *htt*-bipyridinium are worth considering as the first elements of a new family since the R^n peripheral substituents (Figure 1) can be used to further enhance or tune the three types of properties but also to modify the solubility of the EPs or ensure their docking (or anchoring) to other functional components, including surfaces.[52]

Achievements related to electron-accepting properties of *htt*-EPs deserve to be underlined. First, both branched and fused dicationic EPs exhibit a first reduction potential well comparable with the best electrophores commonly used (e.g., $E_{red} = -0.42$ V vs SCE for $\mathbf{1F_{Me}}/\mathbf{2F_{Me}}$). Second, the single bielectronic reduction observed for branched EPs, quaternarized or not (e.g., $E_{red} = -0.59$ V vs SCE for $\mathbf{1B_{Me}}/\mathbf{2B_{Me}}$), is quite unusual and of interest since multielectron manipulation is highly challenging, in particular in the field of artificial photosynthesis, at the final redox-to-chemical conversion step.[53,54] This ability to undergo a single-step, two-electron reduction can be viewed as a functional emergence,[55] which is closely related to the head-to-tail topology of electrophores. Consequently, as unusual two-electron acceptors, branched *htt*-EPs could open a new path to the study and exploitation of multiphoton/multielectron processes.

Lastly, we validated a computational approach that permits one to derive qualitative criteria, not only to predict the possibility to achieve photoinduced biscyclization of interest for synthetic strategies or within the framework of the in situ preparation of intercalating agents (photochemotherapy),[56] for instance, but also to assess the photochemical stability of branched EPs. In this regard, it is worth noting that the most efficient EPs as electrophores (i.e., *N*-alkylated derivatives like $\mathbf{1B_{Me}}/\mathbf{2B_{Me}}$) do not undergo light-triggered pericondensation.

5. Experimental Section

5.1. Syntheses, Characterization, and General Experimental Details. Materials, syntheses of the EPs including general procedures to prepare pyrylium precursors[57] and branched pyridiniums,[58] along with full characterizations are provided in the Supporting Information.

5.2. Electrochemical Measurements. The electrochemical experiments were carried out with a conventional three-electrode cell (solution volume of 15 mL) and a PC-controlled potentiostat/galvanostat (Princeton Applied Research Inc. model 263A). The working electrode was a platinum electrode from Radiometer-Tacussel exposing a geometrical area of 0.034 cm^2 and mounted in Teflon. The electrode was polished before each experiment with 3 and 0.3 μm alumina pastes followed by extensive rinsing with ultrapure Milli-Q water. Platinum wire was used as the counter electrode and saturated calomel electrode, SCE, as reference electrode. Electrolytic solutions, MeCN (Aldrich, anhydrous, 99.8%) containing tetrabutylammonium hexafluorophosphate 0.1 M ($TBAPF_6$, Aldrich, +99%) as supporting electrolyte, were routinely deoxygenated by argon bubbling. All potential values are given versus the calomel saturated electrode SCE. The reported numerical values (Table 1) were corrected by using dissolved Fc^+/Fc couple as an internal reference standard and by setting $E_{1/2}$ (Fc^+/Fc) equal to +0.380 V vs SCE in MeCN.[59] Cyclic voltammetry experiments were conducted at scan rate of 0.1 V s^{-1} (except where specified in the text). Rotating disk electrode voltammetry experiments were conducted at scan rate of 0.01 V s^{-1} by rotating the disk electrode at 2000 rotations per minute (rpm) (Controvit device from Radiometer-Tacussel, France). Square wave voltammetry experiments were performed with a potential sweep rate of 100 mV s^{-1} (pulse height = 25 mV, step height = 2 mV, and frequency = 50 Hz).

5.3. Photophysical Properties. For steady-state luminescence measurements, a Jobin Yvon-Spex Fluoromax P spectrofluorimeter was used, equipped with a Hamamatsu R3896 photomultiplier, and the spectra were corrected for photomultiplier response using a program purchased with the fluorimeter. For the luminescence lifetimes, an Edinburgh OB 900 time-correlated single-photon-counting spectrometer was used. As excitation sources, a Hamamatsu PLP 2 laser diode (59 ps pulse width at 408 nm) and the nitrogen discharge (pulse width, 2 ns at 337 nm) were employed. Emission

(51) Würthner, F. *Chem. Commun.* **2004**, 1564–1573.
(52) Bongard, D.; Möller, M.; Rao, S. N.; Corr, D.; Walder, L. *Helv. Chim. Acta* **2005**, *88*, 3200–3209.
(53) (a) Gust, D.; Moore, T. A.; Moore, A. L. *Acc. Chem. Res.* **2009**, *42*, 1890–1898. (b) Magnuson, A.; Anderlund, M.; Johansson, O.; Lindblad, P.; Lomoth, R.; Polivka, T.; Ott, S.; Stensjö, K.; Styring, S.; Sundström, V.; Hammarström, L. *Acc. Chem. Res.* **2009**, *42*, 1899–1909. (c) Sala, X.; Romero, I.; Rodriguez, M.; Escriche, L.; Llobet, A. *Angew. Chem., Int. Ed.* **2009**, *48*, 2842–2852. (d) Tinker, L. L.; McDaniel, N. D.; Bernhard, S. *J. Mater. Chem.* **2009**, *19*, 3328–3337. (e) Sartorel, A.; Carraro, M.; Scorrano, G.; De Zorzi, R.; Geremia, S.; McDaniel, N. D.; Bernhard, S.; Bonchio, M. *J. Am. Chem. Soc.* **2008**, *130*, 5006–5007. (f) Balzani, V.; Credi, A.; Venturi, M. *ChemSusChem* **2008**, *1*, 26–58. (g) Eisenberg, R.; Gray, H. B. *Inorg. Chem.* **2008**, *47*, 1697–1699. (h) Huyhn, M. H. V.; Meyer, T. J. *Chem. Rev.* **2007**, *107*, 5004–5064. (i) Lewis, N. S.; Nocera, D. G. *Proc. Natl. Acad. Sci. U.S.A.* **2006**, *103*, 15729–15735. (j) McEvoy, J. P.; Brudvig, G. W. *Chem. Rev.* **2006**, *106*, 4455–4483.
(54) (a) Dempsey, J. L.; Brunschwig, B. S.; Winkler, J. R.; Gray, H. B. *Acc. Chem. Res.* **2009**, *42*, 1995–2004. (b) Rau, S.; Schäfer, B.; Gleich, D.; Anders, E.; Rudolph, M.; Friedrich, M.; Görls, H.; Henry, W.; Vos, J. G. *Angew. Chem., Int. Ed.* **2006**, *45*, 6215–6218. (c) Konduri, R.; Ye, H.; MacDonnell, F. M.; Serroni, S.; Campagna, S.; Rajeshwar, K. *Angew. Chem., Int. Ed.* **2002**, *41*, 3185–3187.
(55) Luisi, P. L. *Foundat. Chem.* **2002**, *4*, 183–200.
(56) Di Pietro, M. L.; Puntoriero, F.; Tuyèras, F.; Ochsenbein, P.; Lainé, P. P.; Campagna, S. *Chem. Commun.* **2010**, *46*, 5169–5171.
(57) 2,4,6-Triarylpyrylium tetrafluoroborate salts were prepared by following a modification of the literature methods reported by Moghimi et al. and Wizinger et al. for the synthesis of other 2,4,6-triarylpyrylium salts, see: (a) Moghimi, A.; Rastegar, M. F.; Ghandi, M.; Taghizadeh, M.; Yari, A.; Shamsipur, M.; Yap, G. P. A.; Rahbarnoohi, H. *J. Org. Chem.* **2002**, *67*, 2065–2074. (b) Wizinger, R.; Losinger, S.; Ulrich, P. *Helv. Chim. Acta* **1956**, *39*, 5–15.
(58) Tri- and tetrabranched pyridiniums were synthesized by following a modification of the literature methods reported by Osterby et al., Kessler et al., and Dimroth et al. for the preparation of *N*-phenolate-2,4,6-triarylpyridinium betaine dyes, see: (a) Osterby, B. R.; McKelvey, R. D. *J. Chem. Educ.* **1996**, *73*, 260–261. (b) Kessler, M. A.; Wolfbeis, O. S. *Synthesis* **1988**, 635–636. (c) Dimroth, K.; Reichardt, C.; Siepmann, T.; Bohlmann, F. *Liebigs Ann. Chem.* **1963**, *661*, 1–37.
(59) Pavlishchuk, V. V.; Addison, A. W. *Inorg. Chim. Acta* **2000**, *298*, 97–102.

quantum yields for argon-degassed acetonitrile solutions of the organic species were determined by using the optically diluted method[60] with anthracene in air-equilibrated ethanol solution ($\Phi_{em} = 0.2$) as quantum yield standard.[61] Experimental uncertainties are as follows: absorption maxima, 1 nm; emission maxima, 4 nm; molar absorption values, 10%; luminescence lifetimes, 10%; luminescence quantum yields, 15%.

5.4. Computational Methods. All calculations were carried out at the DFT level using the development version of Gaussian.[62] Unless otherwise specified, a hybrid Hartree−Fock/density functional model, referred to as PBE0, was used.[63] The PBE0 was obtained by casting the PBE exchange and correlation functional[64] in a hybrid DFT/HF scheme, where the HF:DFT exchange ratio is fixed a priori to 1:3.

For the structural optimizations and calculation of the electronic properties, all atoms were described by a double-ζ quality (LANL2) basis set.[65] The molecular structure of each compound was fully optimized.

Optical transitions were computed using the time-dependent DFT approach at the same level of theory. For clarity, only computed transitions with non-negligible oscillator strength ($f \geq 0.02$) are reported in the tables. In this paper only singlet−singlet (i.e., spin-allowed) transitions are discussed. The transitions were computed at least down to 200 nm for all the systems studied. The polarizable continuum model (PCM) of Tomasi and co-workers[66] was applied as an implicit solvation model to simulate solvent effects. More specifically, we used the conductor-like PCM model as implemented in Gaussian code (CPCM). Acetonitrile was considered as the solvent.

In order to simulate fluorescence, the first singlet excited state was relaxed at the CIS level for the branched compounds and at the TD/DFT PBE0 level[67] for the fused analogues.[68] Fluorescence energies were then computed at the TD-DFT level (PBE0) on such optimized structures. Phosphorescence from the triplet state was computed by a ΔSCF approach.

Acknowledgment. I.C., C.A., J.F., F.T., and PPL are grateful to the French National Agency for Research (ANR) "programme blanc" (NEXUS project; No. BLAN07-1_196405). S.C., F.N., and F.P. also acknowledge the University of Messina and PRIN projects for funding. Finally, Dr. V. Marvaud is acknowledged for fruitful discussions and anonymous referees for their constructive suggestions.

Supporting Information Available: Complete refs 12b and 62; experimental details regarding the syntheses and characterizations of new compounds and precursors including ^{1}H NMR (500 MHz) and ^{13}C NMR (126 MHz) spectra as well as ESI-mass spectra; selected cyclic and rotating disk electrode voltammograms; photobiscyclization control experiments; representations of frontier MOs of various EPs; experimental and calculated (TD-DFT) electronic absorption data for EPs as well as computed fluorescence and phosphorescence energies. This material is available free of charge via the Internet at http://pubs.acs.org.

JA108668H

(60) Demas, J. N.; Crosby, G. A. *J. Phys. Chem.* **1971**, *75*, 991–1024.
(61) Dempster, D. N.; Morrow, T.; Quinn, M. F. *J. Photochem.* **1974**, *2*, 329–341.
(62) Frisch, M. J.; et al. *Gaussian DV*, Revision G.01; Gaussian, Inc.: Wallingford, CT, 2009.
(63) Adamo, C.; Barone, V. *J. Chem. Phys.* **1999**, *110*, 6158–6170.
(64) Perdew, J. P.; Burke, K.; Ernzerhof, M. *Phys. Rev. Lett.* **1996**, *77*, 3865–3868.
(65) Dunning, T. H., Jr.; Hay, P. J. In *Modern Theoretical Chemistry*; Schaefer, H. F., III, Ed.; Plenum: New York, 1976; pp 1−28.
(66) Miertus, S.; Scrocco, E.; Tomasi, J. *J. Chem. Phys.* **1981**, *55*, 117–129.
(67) Scalmani, G.; Frisch, M. J.; Mennucci, B.; Tomasi, J.; Cammi, R.; Barone, V. *J. Chem. Phys.* **2006**, *124*, 094107.
(68) Singlet excited states of branched systems have been optimized at the CIS level since they present a more relevant through-space CT character for which the use of structures obtained at the TD-DFT level could be unreliable.